

Clusters of Cavity Solitons Bounded by Conical Radiation

Carles Milián,^{1,*} Yaroslav V. Kartashov,^{1,2} Dmitry V. Skryabin,³ and Lluís Torner^{1,4}

¹*ICFO—Institut de Ciències Fòniques, The Barcelona Institute of Science and Technology, 08860 Castelldefels (Barcelona), Spain*

²*Institute of Spectroscopy, Russian Academy of Sciences, Troitsk, Moscow, 108840, Russia*

³*Department of Physics, University of Bath, Bath BA2 7AY, United Kingdom and ITMO University, St. Petersburg 197101, Russia*

⁴*Universitat Politècnica de Catalunya, 08034 Barcelona, Spain*



(Received 30 May 2018; published 6 September 2018)

We introduce a new class of self-sustained states, which may exist as single solitons or form multisoliton clusters, in driven passive cylindrical microresonators. Remarkably, such states are stabilized by the radiation they emit, which strongly breaks spatial symmetry and leads to the appearance of long polychromatic conical tails. The latter induce long-range soliton interactions that make possible the formation of clusters, which can be stable if their spatial arrangement is noncollinear with the soliton rotation direction in the microcavity. The clusters are intrinsically two dimensional and, also, spatially rich. The mechanism behind the formation of the clusters is explained using soliton clustering theory. Our results bring fundamental understanding of a new class of multidimensional cavity solitons and may lead to the development of monolithic multisoliton sources.

DOI: [10.1103/PhysRevLett.121.103903](https://doi.org/10.1103/PhysRevLett.121.103903)

Introduction.—The advent of suitable materials and experimental techniques to create so-called frequency combs in microring cavities [1,2] triggered an intense research program addressed at exploring the existence of combs that are stable and spectrally broadband. These two features are found together in self-sustained microring cavity solitons (CSs), even in the presence of higher-order linear and nonlinear effects [3–5], affording a continuously renewed source of fundamentally new physical phenomena. One of the most striking discoveries in this context was the existence of frequency locked CSs containing resonant radiation due to higher-order dispersion, first reported in Ref. [6] and further analyzed in Refs. [7–12]. Remarkably, while radiative leaky mechanisms may be detrimental for solitons in conservative systems [13,14], they may play a strong stabilizing role in microring settings [9,10,15,16]. Resonant radiation arises due to the matching of the CS dispersion relation with that of the linear waves on top of the steady state background [9,16–18], and it manifests itself by the appearance of prominent spectral peaks linked to the parent solitons [13,19].

In higher dimensions, CSs are known to exist in the context of monochromatic light [20–23], but they were found to be stable only in a small region of the parameter space if no extra effects, such as stabilizing potentials [24], are considered. By and large, in most of the parameter space strong instabilities and chaos have been shown to occur [25]. Therefore, a fascinating and so far unexplored question arises about whether radiative leakage may stabilize multidimensional micro CSs, taking into account that these are pulses with quite broad spectrum instead of single-color beams.

In this Letter, we show that bright two-dimensional CSs are stabilized in a passive cylindrical microcavity by the

action of the third-order dispersion (TOD). Radiation tails of these CSs are inherently polychromatic as they represent spatiotemporal conical radiation [26]. Various types of conical radiations emitted by nonlinear pulses are routinely observed as transient phenomena in free-space filamentation optics [27–32]. Importantly, radiation bursts emitted *a-periodically* [31,32] can help to arrest collapse [31]. Here we show that conical emission can in fact lock into a complex and strictly stationary CS. Stable two-dimensional CSs with conical tails exist in the parameter domain where CSs with no radiation are highly unstable. Conical radiation sets an intricate landscape for CS interaction that enables the formation of complex cavity soliton clusters (CSCs) containing a finite number of CSs. CSCs are stable only for particular spatial arrangements having no lower-dimensional analogues. Remarkably, spatial structuring as well as dynamical formation of CSCs can be rigorously understood in terms of the presented clustering theory. In addition, instabilities of CSs may be beneficial as they trigger spontaneous formation of CSCs.

Model.—Two-dimensional CSs may exist in cylindrical microcavities, sketched in Fig. 1(b), such as micropillars or microtubes [33–35]. The pump is assumed to excite primarily azimuthal modes with zero group velocity along the vertical coordinate, and therefore, the corresponding Lugiato-Lefever model [36,37] for the intracavity field envelope ψ can be written in the form:

$$-i\partial_t\psi = \frac{1}{2}(B_2\partial_x^2 - 2iB_3\partial_x^3 + \partial_y^2)\psi + (i\gamma - \delta + |\psi|^2)\psi + h, \quad (1)$$

where t , x , and y are, respectively, the normalized time (in round-trip units), the periodic azimuthal coordinate, and the

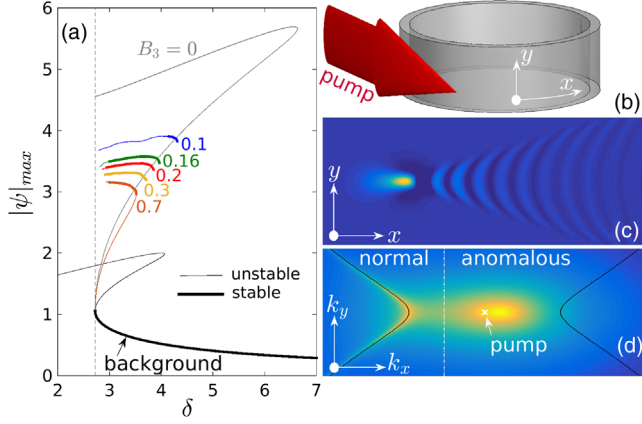


FIG. 1. (a) CS amplitudes versus δ and B_3 (labels at each branch) around the cavity resonance (black) for $h = 2$. Unstable middle branches merging with background are shown only for $B_3 = 0$ and $B_3 = 0.7$. Thick (thin) lines denote stable (unstable) states. (b) Sketch of the driven microcavity. An example of stable soliton is shown in spatial (c) and frequency (d) domains for $B_3 = 0.2$, $\delta = 3.3$. In (d), the vertical line marks the zero GVD and solid curves mark the conical radiation wave numbers calculated from Eq. (2). Pump is at $k_x = k_y = 0$. Axes of panels (c) and (d) are $x \in [-10, 10]$, $y \in [-5, 5]$, $k_x \in [-10, 10]$, $k_y \in [-15, 15]$.

translationally invariant vertical coordinate. $B_2 \equiv \omega^{(2)}\tau / (2\pi R)^2$, $B_3 \equiv \omega^{(3)}\tau / (2\pi R)^3 / 3!$ are the dispersion coefficients; $B_2 > 0$ corresponds to anomalous group velocity dispersion (GVD); $\omega^{(q)} \equiv \partial_{\beta}^q \omega(\beta)|_{\beta_0}$; β is the propagation constant; R is the cylinder radius; γ accounts for losses; $\delta \equiv [\omega_0 - \omega_p]\tau$ is the normalized cavity detuning; ω_p is the pump frequency; ω_0 is the closest resonance to ω_p ; $\tau \equiv 2\pi R n_g / c$ is the round-trip time for the pump frequency; n_g is the group index at ω_p ; $Q = \omega_p \tau / \gamma$ is the quality factor; $\psi = E(\tau n_{\text{NL}})^{1/2}$ and $h = (\tau^3 n_{\text{NL}})^{1/2} \omega_p^2 S / \omega_0$, where E , n_{NL} , S are the physical field, nonlinear coefficient, and coupled pump strength. Equation (1) is invariant under transformations $\{ta, xa^{1/2}, ya^{1/2}, \psi a^{-1/2}, \gamma a^{-1}, \delta a^{-1}, ha^{-3/2}\}$. We set $a = \gamma$ and rescale $x \rightarrow xB_2^{1/2}$ that recasts Eq. (1) with $B_2 = \gamma = 1$. The term $+\partial_y^2 \psi$ excites light with slow vertical motion corresponding to high-order modes of the cylinder cross section near the cutoff frequency where GVD is typically anomalous (hence, the sign $+$) [38–43]. The physical width of the CSCs and that of the pump beam are discussed in the Supplemental Material [44], and are of the order of ~ 1 mm.

Two-dimensional CSs.—Solitons with $B_3 = 0$ are well known in the context of single-color beams and are stable only in a narrow parameter region outside the bistability range [21–23]. In cylindrical microcavities, such two-dimensional solitons are found to be strongly stabilized by the action of TOD, $B_3 \neq 0$ [Fig. 1(a)]. This finding cannot be anticipated by analogy with the one-dimensional case, as the strength and parameter coverage of the soliton

instability increase rapidly in the higher dimensions [45]. Therefore, our result constitutes an important step towards the realization of frequency combs in multidimensional geometries.

A salient feature of the two-dimensional CSs, crucial for this work, comes from the combination of TOD and transverse GVD. As a result, CSs acquire a conical radiation tail, as shown in Figs. 1(c) and 1(d). Such tails fall in the normal GVD regime and therefore resemble free-space optical X waves [46], whose extended tails are interpreted in terms of angular phase matching [26]. In our case, the spectral content of the conical radiation is obtained by requiring phase matching for linear waves $\sim ae^{ik_x x + ik_y y}$ propagating on top of the ψ_0 background away from the soliton core:

$$v_x k_x - B_3 k_x^3 = \pm [(\delta + k_y^2/2 + B_2 k_x^2/2 - |\psi_0|^2)^2 - |\psi_0|^4]^{1/2}, \quad (2)$$

where v_x is the nonzero x component of CS velocity (that we obtain together with soliton profile) induced by TOD. Equation (2) perfectly describes the spectral structure of CS tails, as shown in Fig. 1(d), and in Figs. 3(c) and 3(e) for CSCs.

Theory of CS interaction and dynamical streams.—In order to unveil what types of CSCs exist in cylindrical microcavities, it is crucial to understand how individual CSs form ensembles. To this end, we develop the cluster formation theory, presented below for the case of two interacting CSs (see further details in the Supplemental Material [44]). A pair of CSs will bind together at locations in the xy plane meeting equilibria against intersoliton forces. A superposition of two CSs $\psi_{1,2}$ in the reference frame moving with velocity v_x is accurately described by the ansatz $\psi = \psi_1[x_1(t), y_1(t)] + \psi_2[x_2(t), y_2(t)] + \chi$, where χ is a small correction arising due to interacting CSs offset by a distance $[\Delta x^2 + \Delta y^2]^{1/2}$ ($\Delta x \equiv x_2 - x_1$, $\Delta y \equiv y_2 - y_1$). $\dot{x}_{1,2} \equiv \partial_t x_{1,2}$ is the soliton velocity measured relative to v_x and $\dot{y}_{1,2}$ is the transverse velocity component acquired due to CS interaction. When $\psi_{1,2}$ are far from instability thresholds, χ is most naturally regarded as the superposition of two neutral modes excited due to intersoliton forces [47,48]. Substituting the above ansatz in Eq. (1) one obtains linearized equation for $\chi(x, y)$:

$$\sum_{q=1}^2 [\dot{x}_q \partial_{x_q} + \dot{y}_q \partial_{y_q}] \vec{S}_q = \hat{\mathcal{L}} \vec{\chi} + \vec{\mathcal{K}}, \quad (3)$$

where $\vec{\chi} \equiv [\chi^*, \chi]^\dagger$, $\vec{S}_q \equiv [\psi_q^* - \psi_0^*, \psi_q - \psi_0]^\dagger$, and $\vec{\mathcal{K}}$ contains the terms resulting from the soliton-soliton interactions. Projecting the above equation onto the neutral modes of the operator $\hat{\mathcal{L}}^\dagger(\vec{S}_p)$, $\eta_p^{(1)}$ and $\eta_p^{(2)}$ ($p = 1, 2$), leads to the algebraic system of four equations for the soliton velocities $\hat{A}[\dot{x}_1, \dot{x}_2, \dot{y}_1, \dot{y}_2]^T = \mathbf{b}$. The elements of

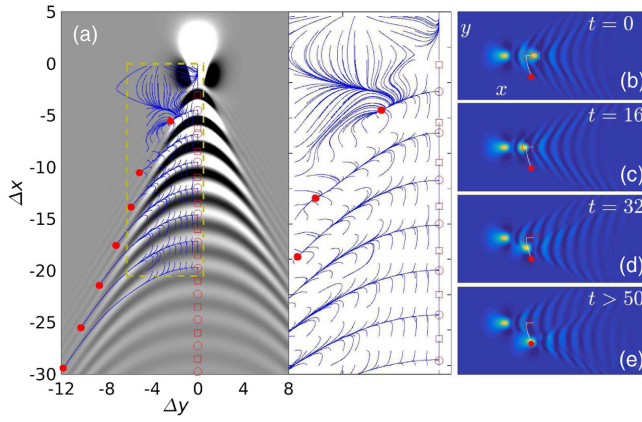


FIG. 2. (a) Theoretically predicted displacements corresponding to two-soliton cluster formation, when one soliton is centered at $\Delta x = \Delta y = 0$ (gray scale background): solid circles denote stable equilibria while hollow circles and squares denote unstable equilibria for the locations of the second soliton (see text). Solid curves show predicted streamlines describing relative motion of the two solitons when initial spatial offsets are within the dashed rectangle. Inset in (a) is an enlargement of the streamlines in the dashed rectangle. (b)–(e) Snapshots corresponding to direct numerical propagation of two-soliton cluster corresponding to unstable equilibrium: $\Delta x = -6.25$, $\Delta y = 0$. White line shows the associated theoretical streamline. Panel sizes, $x \times y$, are 40×10 , $B_3 = 0.7$, $\delta = 3.3$.

the 4×4 matrix \hat{A} and vector \mathbf{b} are, respectively, the projections of $\eta_p^{(1,2)}$ on the neutral modes of $\hat{\mathcal{L}}(\vec{S}_q)$ and on the vector $\vec{\mathcal{K}}$. Two-soliton clusters exist for displacements $\{\Delta x, \Delta y\}$ for which $\Delta v_x \equiv \dot{x}_1 - \dot{x}_2 = 0$ and $\Delta v_y \equiv \dot{y}_1 - \dot{y}_2 = 0$. In addition, such clusters are stable against intersoliton forces only if all velocity vectors $\mathbf{e}_x \Delta v_x + \mathbf{e}_y \Delta v_y$, where $\mathbf{e}_x, \mathbf{e}_y$ are basis vectors, point towards $\{\Delta x, \Delta y\}$ in close proximity of this point.

Figure 2(a) shows predictions of the above theory for two interacting identical single-peak CSs with $B_3 = 0.7$ and $\delta = 3.3$. The reference soliton is plotted on the background. Displacements at which clusters are found are marked by red dots (stable locations) and hollow circles and squares (unstable locations). We show such displacements only for $\Delta y \leq 0$, since the picture is symmetric in Δy . A first result of this analysis is that all collinear states ($\Delta y = 0$) are unstable against intersoliton interactions; thus, our system does not support *stable* analogs of one-dimensional clusters [11,12,49]. Hollow squares correspond to states that are transversely stable but longitudinally unstable, and vice versa for hollow circles. Physically, it seems natural that collinear clusters are unstable because a soliton exposed to the radiation of another one interacts nonlinearly with waves having longitudinal and transverse spread of wave vectors. Therefore, any imbalance in frequency mixing processes will favor longitudinal or transverse displacements. In addition to stable locations (red dots), our theory also provides dynamical insight. The

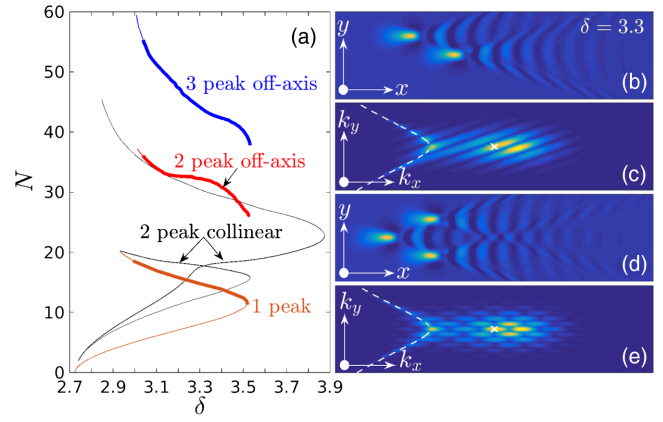


FIG. 3. (a) Norm versus detuning for single CSs and selected clusters of two and three solitons at $B_3 = 0.7$. Thick (thin) curves denote stable (unstable) branches. (b)–(e) Profiles in spatial (b),(d) and frequency (c),(e) domains of stable clusters with two (b),(c) and three (d),(e) solitons at $\delta = 3.3$. Dashed curves in (c) and (e) mark the calculated resonant wave numbers from Eq. (2). Axes are (b),(d) $x \in [-20, 20]$, $y \in [-5, 5]$ and (c),(e) $k_x \in [-6, 6]$, $k_y \in [-12, 12]$.

relative motion of two interacting solitons can be readily predicted by the streamlines of the vector field $\mathbf{e}_x \Delta v_x + \mathbf{e}_y \Delta v_y$. Figure 2(a) shows 250 such streamlines for soliton offsets within the dashed rectangle, which all tend to stable locations.

Stability and dynamical predictions of interacting solitons have been checked extensively via propagation simulations and found excellent agreement. An example is shown in Figs. 2(b)–2(e). In Fig. 2(b) we used as an input at $t = 0$ the exact (computed numerically) collinear two-soliton cluster that was predicted to be unstable against Δx displacements. Because of instability, two peaks approach each other until the state is reached that is unstable only against Δy displacements, Fig. 2(c). Further propagation leads to the displacement [Fig. 2(d)] of the rightmost soliton towards the theoretically predicted stable location [Fig. 2(e)], where it remains from $t = 50$ to huge times $t > 10^4$. Remarkably, the soliton path on the xy plane practically coincides with the theoretical streamline (white solid path). Details on all numerical methods are provided in the Supplemental Material [44].

Clusters of multiple CSs.—In the light of the above results, it is natural to expect very rich families of CSCs in cylindrical microcavities. Figure 3(a) shows selected examples of such families for single-peak CSs and CSCs consisting of two and three CSs. In order to clearly distinguish all families we plot the norm, $N \equiv \iint |\psi(x, y) - \psi_0| dx dy$ versus detuning. Two-CS collinear ($\Delta y = 0$) clusters are seen to bifurcate either from the single-peak solitons or directly from the cavity background. In Fig. 3(a), the latter CSCs have the two CSs with equal amplitudes and thus correspond to the unstable CSCs in Fig. 2.

Branches corresponding to CSCs with noncollinear arrangements are shown in Fig. 3(a) for the cases of two (solid red) and three (solid blue) solitons. Profiles in spatial and frequency domains are shown for $\delta = 3.3$ in Figs. 3(b) and 3(d) and Figs. 3(c) and 3(e), respectively. The two-soliton cluster in Fig. 3(b) corresponds to the equilibrium point $\Delta x = -5.56$ and $\Delta y = -2.40$ in Fig. 2(a). Note that locations $\Delta y = \pm 2.40$ are equally favorable for cluster formation. Populating both of them results in the three-soliton cluster in Fig. 3(d); therefore its structure is also remarkably well predicted by the theory. Noncollinear two-soliton clusters (including their radiative tails) are clearly asymmetric along the y and k_y axes. Hence, transverse recoil effect is possible and leads to the displacement of the spectral maximum associated with soliton into the point with nonzero k_y . Because of this, all transversally asymmetric clusters, like the one in Fig. 2(e), acquire small transverse velocities v_y ($|v_y/v_x| \lesssim 10^{-2}$, see Supplemental Material [44]) that transform circular orbits into helices, leading to transport of light along the cylinder's axis. On the contrary, transversally symmetric clusters, like those in Figs. 2(b), 2(c), and 3(d), have only nonzero longitudinal velocity, v_x , keeping circular orbits.

Instabilities and cluster expansion.—Dynamics of the unstable two-dimensional CSs and CSCs is very rich. Figure 4 illustrates a cascaded process triggered by a single unstable CS at $\delta = 2.95$, shown in Fig. 4(c). Instability in this case first leads to the spontaneous formation of the two-peak collinear state in Fig. 4(d). Such a collinear state is unstable, as predicted, and reshapes into an off-axis pair [cf. Fig. 4(e)]. The rightmost intense part of the radiation front eventually gives birth to a third CS [Figs. 4(f) and 4(g)] that drifts back towards $y = 0$. Because the new CS is born with a small transverse drift with respect to its parent, the drift will necessarily be downside until the predicted

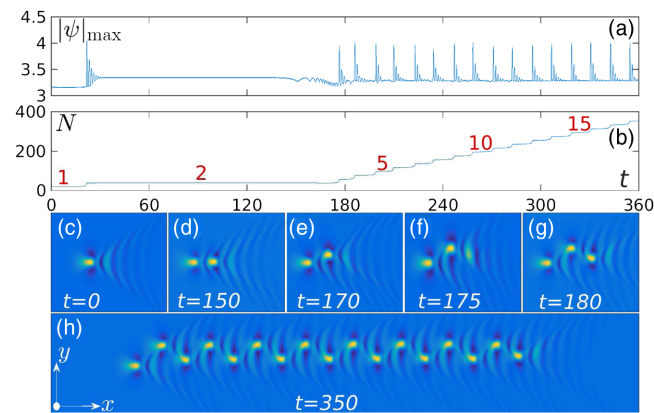


FIG. 4. Temporal evolutions of (a) peak amplitude and (b) norm of the unstable CS at $B_3 = 0.7$, $\delta = 2.95$. Numbers in (b) indicate number of solitons contained in the pattern. (c)–(h) Profiles of the intracavity field for selected times (see labels) illustrating the zigzag cluster formation. Panel sizes ($x \times y$) are (c)–(g) 30×12 and (h) 150×12 .

equilibrium location is reached, in agreement with Fig. 2(a). This cascaded process results in the formation of a zigzag-shaped cluster [Fig. 4(h)]. The appearance of new CSs leads to temporal spikes in peak amplitude and ladder steps in norm, as apparent from Figs. 4(a) and 4(b), respectively. Generation of new CSs is a stimulated process typical when background has inhomogeneities (see, e.g., Refs. [50,51]). This cascaded process is arrested when the pattern extends all over the cavity length or when the detuning is slightly increased and moved into the stability domain for single CSs. While in the former case the pattern becomes chaotic, in the latter case the zigzag cluster breaks into off-axis pairs and single-peak CSs (not shown).

Instabilities may result in spontaneous formation of larger stable CSCs. This is a remarkable dynamical feature of this system, as instabilities, easily triggered via cavity detuning, become beneficial for exciting complex states without the need to construct them from individual CSs placed in predetermined locations. Figures 5(a)–5(d) show an example of this situation, stimulated by an unstable three-peak cluster at $t = 0$ [cf. Fig. 5(a)]. Similarly to dynamics in Fig. 4, the intense radiation peaks stimulate the formation of two new solitons [Fig. 5(b)] that shift towards the center, Fig. 5(c), as dictated by the radiation tails they are exposed to. When they approach each other, as predicted in Fig. 2(a) for $\Delta x = 0$, they start repelling one another and settle into a stable equilibrium. Moreover, their radiation fronts strongly interfere and a sixth soliton appears at the front, locking the ensemble together to form a stable cluster, represented in Fig. 5(d). Interestingly, this complex cluster can be used to form larger stable CSCs, like the 11-peak CSC in Fig. 5(e).

The existence of stable finite-size CSCs formed by optical pulses with extended radiative tails, cf. Figs. 3(b), 3(d), 5(d), and 5(e), having no one-dimensional analogues,

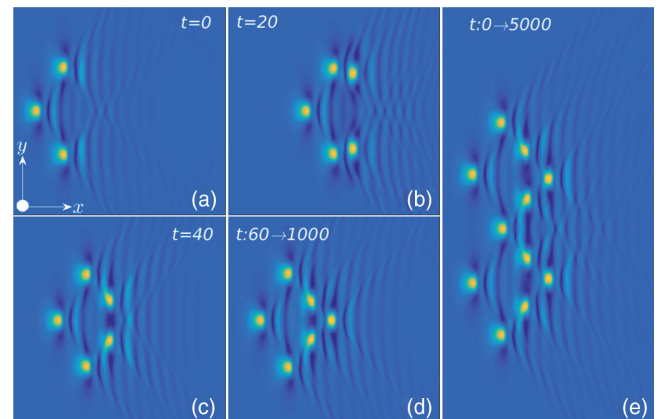


FIG. 5. (a)–(d) Formation of a stable six-peak CSC from an unstable three-peak one: $B_3 = 0.7$, $\delta = 3.02$. (e) Stable 11-peak cluster built from the CSC in (d). Labels indicate temporal instants (a)–(c) or intervals (d),(e) at which profiles are observed. Panel sizes ($x \times y$) are (a)–(d) 50×12 and (e) 50×24 .

is the central result of this Letter. Up to now, stable patterns in Eq. (1) were only known with $B_3 = 0$ and in the form of infinitely extended hexagonal arrangements [52,53]. Our results motivate experimental investigation of suggested structures, which could find applications in multichannel soliton sources, that do not require structuring of dielectric rods into stacks of microrings.

Conclusions.—We introduced a new class of stable multidimensional CSs in monolithic cylindrical microcavities exhibiting pronounced and polychromatic conical radiation tails. We showed that modulations induced by these tails strongly break CS symmetry and draw a complex effective potential ruling interaction of CSs, which can be understood with the presented soliton clustering theory. Equilibrium points were found to exist at *a priori* counter-intuitive spatial locations, leading to intrinsically two-dimensional and highly nontrivial stable clusters with no lower-dimensional analogues. Our results are physically rich and bring fundamental insights into the physics of cavity solitons.

This work was supported by MINECO through the Juan de la Cierva incorporación program, Severo Ochoa program SEV-2015-0522, and Grant No. FIS2015-71559-P; Generalitat de Catalunya, CERCA; Fundació Cellex, Fundació Mir-Puig; The Leverhulme Trust (RPG-2015-456); H2020 (691011, Soliring); RFBR (17-02-00081).

* carles.milian@icfo.eu

- [1] D. K. Armani, T. J. Kippenberg, S. M. Spillane, and K. J. Vahala, *Nature (London)* **421**, 925 (2003).
- [2] T. J. Kippenberg, R. Holzwarth, and S. Diddams, *Science* **332**, 555 (2011).
- [3] V. Brasch, M. Geiselmann, T. Herr, G. Lihachev, M. H. Pfeiffer, M. L. Gorodetsky, and T. J. Kippenberg, *Science* **351**, 357 (2016).
- [4] M. Karpov, H. Guo, A. Kordts, V. Brasch, M. H. P. Pfeiffer, M. Zervas, M. Geiselmann, and T. J. Kippenberg, *Phys. Rev. Lett.* **116**, 103902 (2016).
- [5] Q.-F. Yang, X. Yi, K. Y. Yang, and K. Vahala, *Nat. Phys.* **13**, 53 (2017).
- [6] S. Coen, H. G. Randle, T. Sylvestre, and M. Erkintalo, *Opt. Lett.* **38**, 37 (2013).
- [7] A. V. Cherenkov, V. E. Lobanov, and M. L. Gorodetsky, *Phys. Rev. A* **95**, 033810 (2017).
- [8] M. R. E. Lamont, Y. Okawachi, and A. L. Gaeta, *Opt. Lett.* **38**, 3478 (2013).
- [9] C. Milián and D. Skryabin, *Opt. Express* **22**, 3732 (2014).
- [10] P. Parra-Rivas, D. Gomila, F. Leo, S. Coen, and L. Gelens, *Opt. Lett.* **39**, 2971 (2014).
- [11] P. Parra-Rivas, D. Gomila, P. Colet, and L. Gelens, *Eur. Phys. J. D* **71**, 198 (2017).
- [12] A. G. Vladimirov, S. V. Gurevich, and M. Tlidi, *Phys. Rev. A* **97**, 013816 (2018).
- [13] N. Akhmediev and M. Karlsson, *Phys. Rev. A* **51**, 2602 (1995).
- [14] D. V. Skryabin and A. V. Gorbach, *Rev. Mod. Phys.* **82**, 1287 (2010).
- [15] J. H. Talla Mbé, C. Milián, and Y. K. Chembo, *Eur. Phys. J. D* **71**, 196 (2017).
- [16] D. V. Skryabin and Y. V. Kartashov, *Opt. Express* **25**, 27442 (2017).
- [17] V. I. Karpman, *Phys. Lett. A* **181**, 211 (1993).
- [18] V. V. Afanasjev, C. R. Menyuk, and Y. S. Kivshar, *Opt. Lett.* **21**, 1975 (1996).
- [19] G. Chang, L.-J. Chen, and F. X. Kärtner, *Opt. Express* **19**, 6635 (2011).
- [20] A. J. Scroggie, W. J. Firth, G. S. McDonald, M. Tlidi, R. Lefever, and L. A. Lugiato, *Chaos Solitons Fractals* **4**, 1323 (1994).
- [21] D. Gomila, A. Jacobo, M. A. Matías, and P. Colet, *Phys. Rev. E* **75**, 026217 (2007).
- [22] W. J. Firth, G. K. Harkness, A. Lord, J. M. McSloy, D. Gomila, and P. Colet, *J. Opt. Soc. Am. B* **19**, 747 (2002).
- [23] W. J. Firth and A. Lord, *J. Mod. Opt.* **43**, 1071 (1996).
- [24] G. J. de Valcárcel and K. Staliunas, *Phys. Rev. A* **87**, 043802 (2013).
- [25] K. Panajotov, M. G. Clerc, and M. Tlidi, *Eur. Phys. J. D* **71**, 176 (2017).
- [26] M. Kolesik, E. M. Wright, and J. V. Moloney, *Phys. Rev. Lett.* **92**, 253901 (2004).
- [27] D. Faccio, M. A. Porras, A. Dubietis, G. Tamosauskas, E. Kucinskas, A. Couairon, and P. DiTrapani, *Opt. Commun.* **265**, 672 (2006).
- [28] A. Couairon, E. Gaizauskas, D. Faccio, A. Dubietis, and P. Di Trapani, *Phys. Rev. E* **73**, 016608 (2006).
- [29] M. Durand, K. Lim, V. Jukna, E. McKee, M. Baudelet, A. Houard, M. Richardson, A. Mysyrowicz, and A. Couairon, *Phys. Rev. A* **87**, 043820 (2013).
- [30] T. Roger, M. F. Saleh, S. Roy, F. Biancalana, C. Li, and D. Faccio, *Phys. Rev. A* **88**, 051801(R) (2013).
- [31] P. Panagiotopoulos, P. Whalen, M. Kolesik, and J. V. Moloney, *Nat. Photonics* **9**, 543 (2015).
- [32] C. Brée, I. Babushkin, U. Morgner, and A. Demircan, *Phys. Rev. Lett.* **118**, 163901 (2017).
- [33] N. B. Tomazio, A. J. G. Otuka, G. F. B. Almeida, X. Roselló-Mechó, M. V. Andrés, and C. R. Mendonça, *J. Polym. Sci., Part B: Polym. Phys.* **55**, 569 (2017).
- [34] T. Kipp, H. Welsch, C. Strelow, C. Heyn, and D. Heitmann, *Phys. Rev. Lett.* **96**, 077403 (2006).
- [35] J. Wang, T. Zhan, G. Huang, P. K. Chu, and Y. Mei, *Laser Photonics Rev.* **8**, 521 (2014).
- [36] L. A. Lugiato and R. Lefever, *Phys. Rev. Lett.* **58**, 2209 (1987).
- [37] Y. K. Chembo and C. R. Menyuk, *Phys. Rev. A* **87**, 053852 (2013).
- [38] A. V. Yulin and D. V. Skryabin, *Opt. Lett.* **31**, 3092 (2006).
- [39] J. Laegsgaard, *J. Opt. Soc. Am. B* **28**, 37 (2011).
- [40] J. Laegsgaard, *J. Opt. Soc. Am. B* **28**, 2617 (2011).
- [41] I. Oreshnikov and D. V. Skryabin, *Opt. Express* **25**, 10306 (2017).
- [42] S. V. Suchkov, M. Sumetsky, and A. A. Sukhorukov, *Opt. Lett.* **42**, 2149 (2017).
- [43] Y. V. Kartashov, M. L. Gorodetsky, A. Kudlinski, and D. V. Skryabin, *Opt. Lett.* **43**, 2680 (2018).

- [44] See Supplemental Material at <http://link.aps.org/supplemental/10.1103/PhysRevLett.121.103903> for details on numerical methods, perturbation theory around Eq. (3), cavity dispersion, and physical soliton widths.
- [45] We scanned intensively the parameter space in 3D, i.e., replacing $\partial_y^2 \rightarrow \partial_y^2 + \partial_z^2$ in Eq. (1), and found that all radiating bullets with radial symmetry were clearly unstable.
- [46] C. Conti, S. Trillo, P. Di Trapani, G. Valiulis, A. Piskarskas, O. Jedrkiewicz, and J. Trull, *Phys. Rev. Lett.* **90**, 170406 (2003).
- [47] A. G. Vladimirov, J. M. McSloy, D. V. Skryabin, and W. J. Firth, *Phys. Rev. E* **65**, 046606 (2002).
- [48] D. V. Skryabin and W. J. Firth, *Opt. Lett.* **24**, 1056 (1999).
- [49] Y. Wang, F. Leo, J. Fatome, M. Erkintalo, S. G. Murdoch, and S. Coen, *Optica* **4**, 855 (2017).
- [50] P. Parra-Rivas, D. Gomila, M. A. Matías, P. Colet, and L. Gelens, *Opt. Express* **22**, 30943 (2014).
- [51] C. Milián, A. V. Gorbach, M. Taki, A. V. Yulin, and D. V. Skryabin, *Phys. Rev. A* **92**, 033851 (2015).
- [52] W. J. Firth, A. J. Scroggie, G. S. McDonald, and L. A. Lugiato, *Phys. Rev. A* **46**, R3609(R) (1992).
- [53] M. Tlidi, R. Lefever, and P. Mandel, *Quantum Semiclass. Opt.* **8**, 931 (1996).